



Cite this: *RSC Adv.*, 2023, **13**, 19881

Received 19th April 2023
 Accepted 14th June 2023

DOI: 10.1039/d3ra02607h
rsc.li/rsc-advances

Highly efficient and selective CO₂ capture of Li₂CO₃- and (Li-K)₂CO₃-based porous carbon composites†

Honghao Li and Tuerxun Nasiman  *

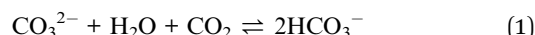
In this study, Li₂CO₃- and (Li-K)₂CO₃-based porous carbon composites were synthesized from terephthalic acid, lithium hydroxide and sodium hydroxide through calcination at different temperatures. These materials were fully characterized through X-ray diffraction, Raman spectroscopy, and nitrogen adsorption and desorption. Results showed that the excellent CO₂ capture capacities of LiC-700 °C and LiKC-600 °C were 140 and 82 mg CO₂ g⁻¹ at 0 °C and 25 °C, respectively. Additionally, it is calculated that the selectivity of LiC-600 °C and LiKC-700 °C with a CO₂/N₂ (15 : 85) mixture was about 27.41 and 15.04, respectively. Therefore, Li₂CO₃- and (Li-K)₂CO₃-based porous carbon materials could be used to effectively capture CO₂ with high capacity and high selectivity.

1 Introduction

Over the past few decades, excessive human-caused carbon dioxide (CO₂) emissions, such as the combustion of fossil fuels and their derivatives, have been identified as the main cause of the greenhouse effect, ocean acidification and related climate change.^{1,2} According to the latest data from the Mauna Loa Observatory in August 2021,³ the current level of CO₂ in the atmosphere has reached up to 416 ppm, which is nearly 200 ppm higher than that of the pre-industrial period, and far exceeds the consumption capacity of plants in the natural carbon cycle. Therefore, it is very important, even urgent that we reduce carbon emissions for human health.^{4,5} Although there have been many studies on converting fossil fuels that produce CO₂ into renewable clean energy, the capture and storage of carbon dioxide is still believed to be the fastest and most effective solution to reduce the current emission levels in the use of fossil fuel-based power plants (usually coal-based ones). To date, there are many important and cost-effective post-combustion CO₂ capture methods, such as modified amine solution absorption, solid adsorption and membrane separation. In order to have excellent adsorption reversibility, adsorbent recyclability and adsorption efficiency, adsorbents must have large specific surface area, high selectivity and high cycle stability.⁶

Recently, solid alkali metal carbonate adsorbents have attracted more and more attention in the CO₂ capture due to their higher capture capacity and low cost than those of others.

For example, Na₂CO₃ was reported as a good CO₂ adsorbent under (0.1 MPa at >313 K).^{7,8} Results showed that humidity played a critical role in CO₂ capture capacity and the overall reaction rate. With the increase of H₂O concentration, both the rate and amount of captured CO₂ were increased significantly, because carbonate could capture CO₂ under humid conditions to generate bicarbonate (eqn (1)). After the CO₂ capture, the adsorbent could be regenerated and recycled after the decomposition of bicarbonate at 100–200 °C (reverse reaction of eqn (1)).⁹



Theoretically, the CO₂ adsorption capacities of commercial Na₂CO₃ and K₂CO₃ were 41.5 wt% and 31.8 wt%, respectively.¹⁰ According to the thermogravimetric analysis from Luo *et al.*,¹¹ with high CO₂ and H₂O concentrations, pure Na₂CO₃ reacted with CO₂ and H₂O to form NaHCO₃ directly. However, with low CO₂ and H₂O concentrations, Na₂CO₃ preferentially reacted with H₂O to generate Na₂CO₃·H₂O, and this hydrate slowly reacted with CO₂ to produce Na₅H₃(CO₃)₄, which finally slowly reacted with CO₂ and H₂O to form NaHCO₃. Additionally, Cai *et al.*,¹² basing on density functional theory and molecular dynamics simulation, studied the adsorption process and adsorption types of CO₂ and H₂O on Na₂CO₃ crystal surfaces from the atomic scale. Their results showed that the carbonation reaction rate of Na₂CO₃ was not controlled by the kinetics of the surface reaction, was controlled by the phase diffusion of the adsorbent.

Typically, pure carbonate adsorbents have low cost, low energy consumption, high stability, *etc.*, and are widely used in the petrochemical industry. However, the reaction between carbonate and CO₂ is slow, and special operation equipment is

College of Chemistry and Chemical Engineering, Xinjiang Normal University, Urumqi, 830054, China. E-mail: 384546761@qq.com

† Electronic supplementary information (ESI) available. See DOI: <https://doi.org/10.1039/d3ra02607h>



required, which increase the cost significantly. In practical applications, other materials (such as activated carbon, MgO , zeolite molecular sieve, *etc.*) have been added to combine with the adsorbent,¹¹ which can not only increase the adsorption rate and reduce the regeneration temperature, but also increase the CO_2 adsorption capacity. For example, the regeneration temperature of Na_2CO_3 -carbon nanocomposite (NaC-NC) was lower than that of Na_2CO_3 , the CO_2 capture capability of NaC-NC was also higher with a higher reaction rate that was 1.5 to 2 times that of untreated Na_2CO_3 . When K_2CO_3 -carbon composite (KC-CC) was used instead of NaC-NC, a slightly smaller CO_2 amount was captured with a lower regeneration temperature¹³.

In this study, in order to have high adsorption capacity and adsorption rate, Li_2CO_3 -based porous carbon materials were prepared from terephthalic acid and lithium hydroxide. With the added KOH to these same raw materials, $(\text{Li}-\text{K})_2\text{CO}_3$ -based porous carbon materials were further synthesized. With Li_2CO_3 - and $(\text{Li}-\text{K})_2\text{CO}_3$ -based porous carbon materials, the CO_2 capture performance and cycle stability of these materials were significantly improved, and their regeneration temperature was also reduced.

2 Experimental

2.1 Sample preparation

2.1.1 Syntheses of Li_2CO_3 -based porous carbon materials. Terephthalic acid (TPA, McLean), lithium hydroxide and potassium hydroxide were used as raw materials. $\text{LiOH} \cdot \text{H}_2\text{O}$ (0.2 mol, 8.39 g) and TPA (0.1 mol, 16.61 g) were dissolved in distilled water (200 mL) and stirred magnetically for 2 h. Solvent was removed in a water bath at 80 °C to obtain a white powder. The as-obtained white powder was divided into three portions, which were carbonized in a tube furnace with a high purified N_2 flow (150 mL min⁻¹) at 600 °C, 700 °C and 800 °C, respectively. The holding time was 2 h and the heating rate was 10 °C min⁻¹. After these as-carbonized samples were fully ground, they were labeled with LiC-X °C (X is the calcination temperature). For example, LiC-700 °C indicates LiC with a calcination temperature of 700 °C.

2.1.2 Syntheses of $(\text{Li}-\text{K})_2\text{CO}_3$ -based porous carbon materials. Similarly, with $\text{LiOH} \cdot \text{H}_2\text{O}$ (8.39 g), terephthalic acid (16.61 g) and KOH (5.63 g) as the raw materials, three uniform fine powders (black), labeled as LiKC-X (X represents the calcination temperature) were obtained.

2.2 Characterization of materials

The XRD pattern was collected on a Rigaku Smartlab SE X-ray diffractometer from Japan, with a Cu target, a $\text{K}\alpha$ radiation source, $\lambda = 1.5418$ nm, a tube voltage of 40 kV, and a tube current of 40 mA. The weight loss process of the material was recorded on a German Netzsch STA 449 F3 thermogravimetric analyzer under a N_2 atmosphere (20 mL min⁻¹) and a heating rate of 10 °C min⁻¹. The sorbent was analyzed using a high-resolution field emission scanning electron microscope (SEM), Zeiss sigma300 surface topography and structure, the

acceleration voltage was 3 kV. The Raman analysis was done on a HORIBA Scientific LabRAM HR Evolution spectrometer. At room temperature, the laser wavelength of 514 nm was used with the wavenumber range of 800–2000 cm⁻¹. The adsorption and desorption isotherms of CO_2 and N_2 were measured using an adsorption instrument (ASAP 2460, Micromeritics Instrument Co., Ltd., USA). The specific surface area was calculated according to the Brunauer–Emmett–Teller (B–E–T) method. The pore volume (V_{pore}) and pore size (D_{pore}) distribution were calculated according to the Barrett–Joyner–Halenda (B–J–H) formula. The number and strength of basic sites on the surface of the adsorbent were CO_2 determined through temperature-programmed desorption (CO_2 -TPD) on a chemisorption instrument (AutoChem II 2920, Micromeritics Instruments, Inc., USA).

2.3 Adsorption test

2.3.1 CO_2 adsorption–desorption isotherm. After the sample (approximately 0.1 g) was degassed in vacuum at 200 °C for 4 h, its CO_2 adsorption isotherms were measured at 0 °C and 25 °C on an ASAP 2460 adsorption analyzer from Micromeritics. The CO_2 adsorption per gram of sample at 0 °C and 25 °C in the pressure range of 0.01–1 bar was then calculated from the adsorption isotherms. The CO_2 adsorption cycles were studied by desorbing adsorbed CO_2 in each adsorption cycle at 473 K for 6 h in a vacuum.

2.3.2 CO_2/N_2 adsorption selectivity. According to the ideal adsorption theory (IAST) and the adsorption capacity of CO_2 and N_2 under the same conditions, adsorption selectivity of the material to CO_2/N_2 mixed gas was calculated as the following eqn (2).

$$S = \frac{q_1/q_2}{p_1/p_2} \quad (2)$$

in which, q_1 and q_2 represent the adsorption amounts of component 1 (CO_2) and 2 (N_2) in the mixed gas, respectively. In this process, the ratio of CO_2/N_2 was set to 15/85 as the classical theoretical composition ratio of flue gas.

2.3.3 Equivalent heat of CO_2 adsorption (Q_{st}). After the amount of CO_2 adsorption per gram sample at different temperatures was obtained from the adsorption isotherm, equivalent heat of CO_2 adsorption (Q_{st}) of the adsorbent at 0 and 25 °C were calculated according to the following Clausius–Clapeyron equation (eqn (3)) as,

$$Q_{\text{st}} = -RT^2 (\partial \ln P / \partial T)_q \quad (3)$$

where, P is the equilibrium pressure, q is the adsorption amount, T is the absolute temperature, and R is the universal gas constant.

3 Results and discussion

3.1 Characterization

The XRD patterns of Li_2CO_3 -based porous carbon materials prepared at three different calcination temperatures of 600, 700 and 800 °C were shown in Fig. 1. Their diffraction peaks were



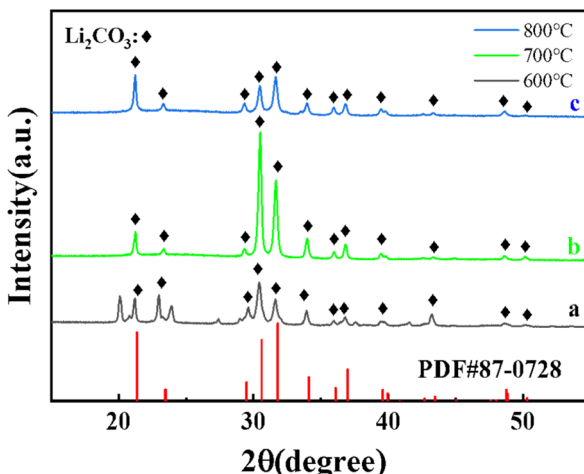


Fig. 1 XRD patterns of LiC-800 °C (a), LiC-700 °C (b) and LiC-600 °C (c). ◆: Li_2CO_3 .

basically consistent with the lithium carbonate standard card PDF#87-0728. When the calcination temperature was 700 °C, the peak intensity of Li_2CO_3 was the highest, indicating the highest crystal phase content at 700 °C. The lithium carbonate was from the carbonation of lithium terephthalate, because terephthalate reacted with lithium hydroxide in solution to generate lithium terephthalate whose chemical bonds in the benzene ring and carboxyl group could be broken at high temperature to form CO_2 , H_2O , amorphous carbon and Li_2CO_3 . Fig. 2 shows XRD patterns of $(\text{Li}-\text{K})_2\text{CO}_3$ -based porous carbon materials prepared at three different calcination temperatures of 600, 700 and 800 °C. The diffraction peaks in the patterns were mainly from LiKCO_3 (PDF#88-0341) and Li_2CO_3 (PDF#87-0729). When the calcination temperature was 600 °C, the crystal phase was more stable with higher crystal phase content than those from other temperatures. Further increasing the calcination temperature would lead to more unstable impurity phases with lower peak intensity. Due to the better purity of

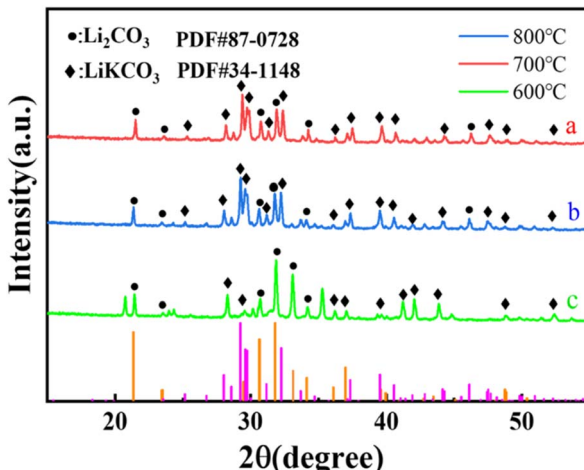


Fig. 2 XRD patterns of LiKC-800 °C (b), LiKC-700 °C (a) and LiKC-600 °C (c). ◆: LiKCO_3 , ●: Li_2CO_3 .

these samples, we further considered LiC-700 °C and LiKC-600 °C.

Fig. 3 shows the thermogravimetric curve of LiC-700 °C under a nitrogen atmosphere. This Li_2CO_3 -based porous carbon material had a small weight loss between room temperature and 624.31 °C, mainly due to the adsorbed water vapor and CO_2 from the air. There was a significant weight loss of about 45% from 624.31 °C to 820.55 °C because of the loss of the volatile substances through oxidization. As shown in Fig. 3b, the LiKCO_3 -based porous carbon material only had a small amount of weight loss from 108.33 °C to 184.62 °C, mainly due to the adsorbed impurities such as water vapor and CO_2 from the air. The significant weight loss of about 60% from 596.37 °C to 973.13 °C came from the carbonization of material. Fig. 3(c) and (d) showed the weight loss processes of LiC and LiKC material at three calcination temperatures. It was found that the material synthesized at 800 °C was the fastest to lose the weight at the beginning. When the temperature was increased to 900 °C, LiC-600 °C and LiKC-800 °C materials had the lowest ash content.

Fig. 4 shows SEM images of materials LiC-700 °C and LiKC-600 °C. The irregular porous particle structure on their surface could be clearly observed, which might increase their specific surface area.

As shown in Fig. 5, the two Raman characteristic peaks at 1350 and 1590 cm^{-1} corresponded to the G band and D band, respectively. The D band indicated the degree of disorder of the amorphous carbon and the defects of the graphite phase, and the G band was due to the bending vibration of sp^2 hybridized graphite phase carbon atoms. Relative intensity (I_D/I_G) of the two peaks indicates the density of defects or the degree of graphitization and a high ratio means high defectivity. With the addition of KOH, the value of I_D/I_G was increased from 0.92 to 0.99, indicating that the addition of KOH increased the number of defects in the carbon skeleton of LiKC-600 °C.

Fig. 6 shows the N_2 adsorption-desorption isotherms and pore size distribution diagrams of these materials, and Table 1

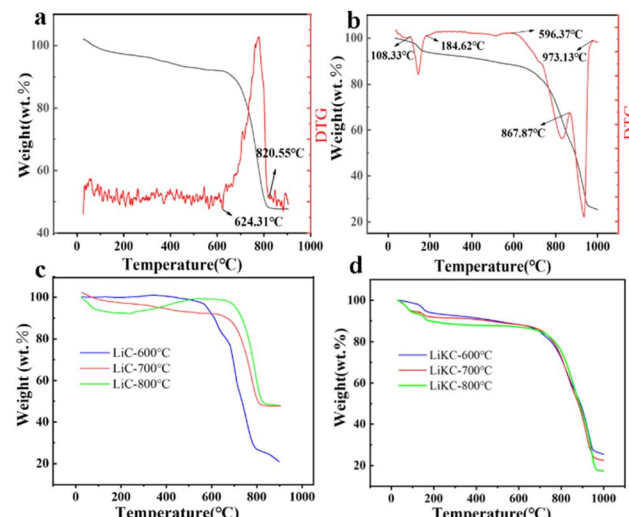


Fig. 3 Thermogravimetric curves of LiC-700 °C (a) and LiKC-600 °C (b), and thermogravimetric curves of materials with calcination temperatures (c and d).

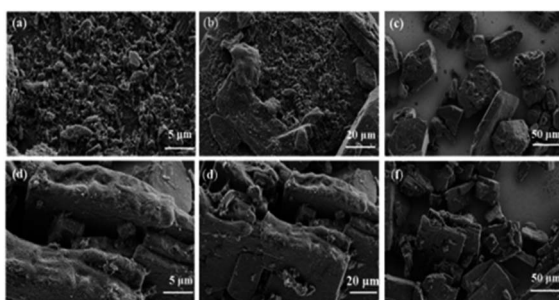


Fig. 4 SEM images of LiC-700 °C (a–c) and LiKC-600 °C (d–f).

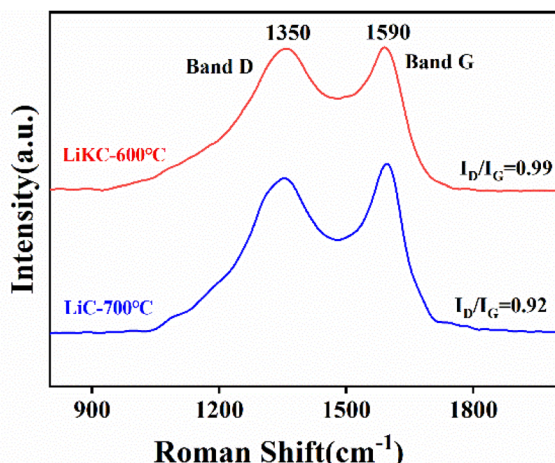


Fig. 5 Raman spectra of LiC-700 °C and LiKC-600 °C.

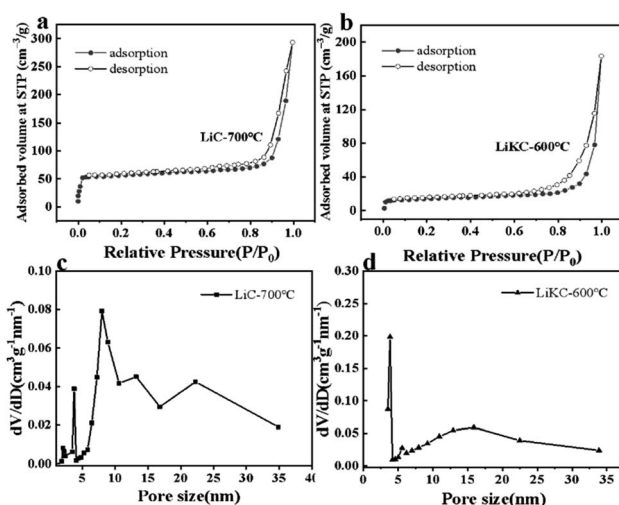


Fig. 6 N₂ adsorption-desorption isotherms of LiC-700 °C (a) and LiKC-600 °C (b), and pore size distributions of LiC-700 °C (c) and LiKC-600 °C (d).

lists their structural properties. They were all type IV isotherms, indicating they were all mesoporous. Typically, the adsorption properties of mesoporous materials are determined by the adsorbent-adsorbed species interactions, as well as the

Table 1 Structure data of LiC and LiKC

Adsorbent	S_{BET} ($\text{m}^2 \text{ g}^{-1}$)	V_{total} ($\text{cm}^3 \text{ g}^{-1}$)	Pore size (nm)
LiC-600 °C	136.1	0.18	14.1
LiC-700 °C	320.0	0.27	20.6
LiC-800 °C	124.4	0.28	17.4
LiKC-600 °C	126.8	0.15	15.4
LiKC-700 °C	23.1	0.06	15.8
LiKC-800 °C	7.5	0.05	15.4

interactions between molecules in the condensed state. In these mesopores, the initial monolayer–multilayer adsorption on the mesoporous walls follows the corresponding partial path of the type II isotherm. However, subsequent condensation can occur within the pore. During the desorption process, a hysteresis loop can be formed due to capillary condensation. Based on the pore size distribution diagrams these two materials (LiC-700 °C and LiKC-600 °C) were dominated by mesopores, and their pore structure data could be calculated according to the adsorption isotherm as listed in Table 1. The specific surface area of LiKC-600 °C was $320.0 \text{ m}^2 \text{ g}^{-1}$, and that of LiKC-600 °C was $126.8 \text{ m}^2 \text{ g}^{-1}$. Their pore volumes were $0.27 \text{ cm}^3 \text{ g}^{-1}$ and $0.145 \text{ cm}^3 \text{ g}^{-1}$ with the average pore diameters of 20.6 nm and 15.4 nm, respectively. Fig. S1(a)–(d) and S2(a), (b)† show the N_2 adsorption and desorption isotherm data and pore size distribution of other materials. Data showed that the pore volume and specific surface area of other materials were lower.

The CO_2 -TPD experiment was done to study the effect of adsorbent surface alkalinity on its CO_2 adsorption performance. As shown in Fig. 7, both of these two samples had two CO_2 desorption peaks in the temperature range of 50–500 °C. The α peak at 100–250 °C was a strong desorption peak, and these strong basic sites could improve their CO_2 adsorption performance. The β peak at 300–450 °C was a weak desorption peak due to the adsorption of CO_2 by weak alkaline sites on the surface of the adsorbent. Both the strength and number of basic sites of LiC-700 °C were larger than those of LiKC-600 °C, and the significant α peak indicated that the increase in the number and strength of basic sites was beneficial to the adsorption of acid gas CO_2 . Based on the specific surface area and XRD characterization results of these materials, they should be excellent candidates as adsorbents in the CO_2 adsorption process.

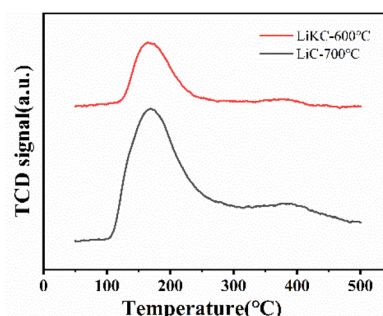


Fig. 7 TPD diagrams of LiC-700 °C and LiKC-600 °C.



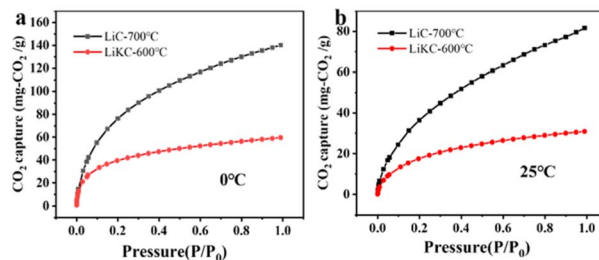


Fig. 8 CO₂ adsorption isotherms at 0 °C (a) and 25 °C (b) of LiC-700 °C and LiKC-600 °C under a pressure from 0.01 to 1 bar.

3.2 CO₂ adsorption properties of composites

The ASAP-2460 adsorption analyzer was used to evaluate the CO₂ adsorption performance of the as-prepared sorbents. CO₂ isothermal adsorption curves at 0 and 25 °C were shown in Fig. 8. Fig. 8(a) and (b) shows that the largest CO₂ adsorption capacity of LiC-700 °C reached up to 140 and 82 mg CO₂ g⁻¹ at 0 and 25 °C under 1 bar, respectively. However, the CO₂ adsorption capacity of LiKC-600 °C was relatively low under 1 bar as 60 and 31 mg CO₂ g⁻¹ at 0 and 25 °C, respectively. Results showed that all isothermal adsorption curves at different temperatures had the same trend, and the CO₂ adsorption isotherms at 0 °C were generally higher than those at 25 °C.

According to adsorption isotherms of these two materials at different temperatures in Fig. 8(a) and (b), the addition of potassium hydroxide in the preparation process decreased their CO₂ adsorption capability, while more suitable calcination temperature led to better CO₂ adsorption performance. These results indicated that treatment at 700 °C led to both larger pore size and larger specific surface area (as evident from Table 1), which further resulted in greater CO₂ adsorption. In order to investigate the CO₂ adsorption selectivity, the CO₂ and N₂ adsorption isotherms were measured (under the 1 bar at 25 °C) for LiC-600 °C and LiKC-700 °C samples as shown in Fig. 9(a) and (b), respectively. It was found that the CO₂ adsorption capacity of LiC-600 °C and LiKC-700 °C was significantly higher than that of N₂, indicating that these materials could carry out significant selective adsorption in the binary gas mixture of CO₂ and N₂. Based on these two adsorption isotherms, the ideal adsorption solution theory (IAST) was used to explore the selectivity of CO₂/N₂. According to formula (3), it is calculated that the selectivity of LiC-600 °C and LiKC-700 °C with a CO₂/N₂

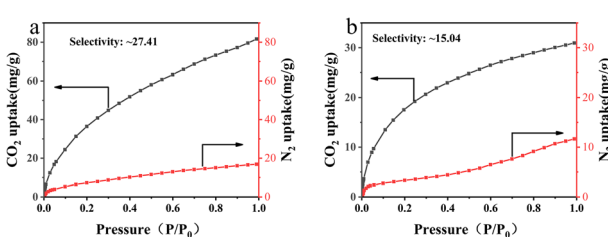


Fig. 9 CO₂ and N₂ adsorption isotherms of LiC-600 °C (a) and LiKC-700 °C (b) at 25 °C under 1 bar.

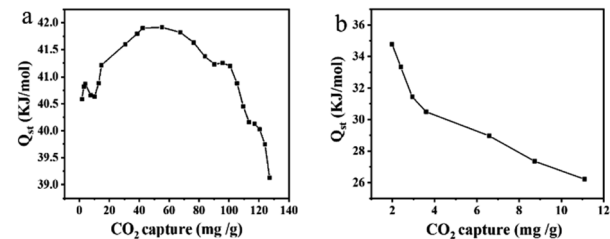


Fig. 10 Q_{st} of equal adsorption heat for LiC-700 °C (a) and LiKC-600 °C (b).

(15 : 85) mixture was about 27.41 and 15.04, respectively. These results showed that LiC-600 °C and LiKC-700 °C had excellent selective adsorption of CO₂ in gas mixtures with a great potential in gas separation.

Generally, the equivalent adsorption heat (Q_{st}), which can be calculated according to the Clausius–Clapeyron equation, reflects the ability of CO₂ molecules to bind to the adsorbent, and a higher value indicates a stronger interaction and a more stable adsorption. As shown in Fig. 10, the initial Q_{st} values of LiC-700 °C and LiKC-600 °C were 40.5 and 34.8 kJ mol⁻¹, respectively, and the Q_{st} values were decreased significantly with the increase of CO₂ adsorption, probably due to the gradual decrease of the interaction between the reaction site and CO₂. In addition, the Q_{st} value of LiKC-600 °C was 34.8 kJ mol⁻¹, which was lower than the binding energy of a typical covalent bond, indicating that the CO₂ adsorption might be a typical physical adsorption, which made the adsorbent regeneration process simple and energy efficient. All results showed that these materials were great candidates to capture CO₂ with a low regeneration energy consumption and low regeneration cost.

Table 2 shows the CO₂ adsorption capacity and CO₂/N₂ adsorption selectivity of the LiC-600 °C, LiKC-700 °C, and some other reported adsorbents. These results showed that the MOF material had a higher CO₂ adsorption capacity and selectivity than other adsorbents, and Cu-BTC had a significantly higher adsorption capacity. However, due to the high cost and poor

Table 2 Comparison of CO₂ adsorption capacity at 100 kPa and CO₂/N₂ adsorption selectivity at 100 kPa of different adsorbents

Adsorbents	Adsorption capacity (mmol g ⁻¹) 100 kPa	CO ₂ /N ₂ selectivity	Ref.
Cu-BTC	4.79 (298 K)	~50	14
MIL-101 (Cr)	2.33 (298 K)	~20	15
MIL-100 (Fe)	2.25 (298 K)	6	16
Zeolite Y	0.73 (303 K)	11	17
20MgO/MCN	1.15 (298 K)	—	18
ZSM-5	1.33 (298 K)	~8	19
AC ₂ TMAOH	2.49 (303 K)	31.53	20
Commercial AC	1.5 (298 K)	—	21
Zeolite 13×	4.20 (298 K)	130	22
LiC-700	3.18 (273 K) 1.86 (298 K)	— ~27.45	This study
LiKC-600	1.36 (273 K) 0.70 (298 K)	— ~15.04	This study



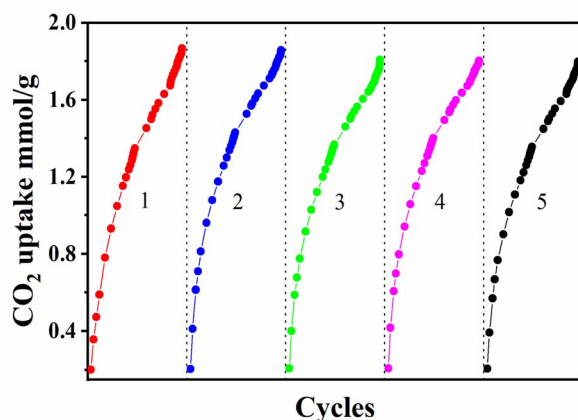


Fig. 11 Five cycles of CO_2 adsorption capacity for LiC-700 °C at 25 °C.

durability and mechanical strength of MOF materials, their application in industry was still very rare up to present. Compared with the other molecular sieve and AC adsorbents in Table 2, the LiC-700 °C adsorbents in this study showed both a higher CO_2 adsorption capacity and a higher CO_2/N_2 adsorption selectivity, except of the 13 \times molecular sieve and modified activated carbon AC2_{TMAOH}. However, carbon material adsorbents had important advantages over zeolite 13 \times such as hydrophobicity, which could significantly reduce the cost with a lower energy required for regeneration.²³ This work mainly focuses on providing a simple method for the preparation of LiC adsorbents and to evaluate the effect of introducing alkali metal ions into LiC support on CO_2 adsorption performance. In our future work, in order to improve the CO_2 adsorption capacity of LiC adsorbent, further exploration will be done to optimize the matrix and pore structure of the adsorbent.

In addition to high CO_2 adsorption capacity and selectivity, regeneration is also a key factor for the practical application of CO_2 adsorbent materials. The adsorbent was degassing for 6 hours at under the ambient pressure at 200 °C, the CO_2 adsorption and desorption cyclic experiment was carried out several times to examine the recycling ability of the material. The LiC-700 °C cyclically tested five times at 25 °C. As shown in Fig. 11, after five times regeneration tests, the capacity of the adsorbent did not change substantially. Therefore, it can be speculated that the porous material has a great application prospect in the field of CO_2 adsorption.

4 Conclusions

In this study, with terephthalic acid as a carbon source, Li_2CO_3 - and (Li-K) 2CO_3 -based porous carbon materials were successfully prepared with different alkalis added and different calcination temperatures. Results showed that the optimum calcination temperature of LiC-based carbon materials was around 700 °C, while the optimum calcination temperature of LiKC-based porous carbon materials was around 600 °C. The CO_2 capture capacity of LiC-700 °C was 140 mg $\text{CO}_2 \text{ g}^{-1}$ and that of the LiKC-600 °C also reached up to 64 mg $\text{CO}_2 \text{ g}^{-1}$ at 0 °C (273

K) under 1 bar, respectively. With carbonate doping and high-temperature calcination, the CO_2 capture capacity of these materials could be further improved to a certain high level. The selectivity of LiC-600 °C and LiKC-700 °C with a CO_2/N_2 (15 : 85) mixture was about 27.41 and 15.04, respectively. These results showed that adsorbent had excellent selective adsorption of CO_2 in gas mixtures. According to the CO_2 -TPD analysis, this high selectivity to CO_2 was due to the interaction between the large number of basic sites inside these materials and the acidic CO_2 . Overall, the LiC-700 °C had excellent CO_2 adsorption, selectivity and regeneration. The Li_2CO_3 -based porous carbon exhibit a favorable application prospect in post-combustion CO_2 carbon adsorption and separation.

Author contributions

The manuscript was written through contributions of all authors. All authors have given approval to the final version of the manuscript.

Conflicts of interest

The authors declare no competing financial interest.

Acknowledgements

The study was supported by the Open Project of Xinjiang Key Laboratory of Energy Storage and Photoelectrocatalytic Materials and Introduction plan for 100 young doctors in Xinjiang Uygur Autonomous Region.

Notes and references

- 1 N. Nityashree, G. V. Manohara, M. M. Maroto-Valer and S. Garcia, *ACS Appl. Mater. Interfaces*, 2020, **12**, 33765–33774.
- 2 S. Dutta, A. Bhaumik and K. C. W. Wu, *Energy Environ. Sci.*, 2014, **7**, 3574–3592.
- 3 R. S. Liu, X. U. Shuang, G. P. Hao and L. U. An-Hui, *Chem. Res. Chin. Univ.*, 2022, **38**, 18–30.
- 4 R. Soldi, S. Cavallini, J. Friedl, M. Volpe and C. Zuccaro, *A New Skills Agenda for Europe*, Brussels, 2014.
- 5 *Climate Change 2007: The Physical Science Basis. Contribution of Working Group I to the Fourth Assessment Report of the Intergovernmental Panel on Climate Change*, ed. S. Solomon, D. Qin, M. Manning, Z. Chen, M. Marquis, K. Avery, M. Tignor and H. Miller, Cambridge University Press, 2007, vol. 1.
- 6 Q. Liu, Y. Shi, W. Zhong and A. Yu, *Chin. J. Chem. Eng.*, 2019, **27**, 2261–2272.
- 7 Y. Liang, D. P. Harrison, R. P. Gupta, D. A. Green and W. J. McMichael, *Energy Fuels*, 2004, **18**, 569–575.
- 8 R. R. Kondakindi, G. McCumber, S. Aleksic, W. Whittenberger and M. A. Abraham, *Int. J. Greenhouse Gas Control*, 2013, **15**, 65–69.
- 9 Y. Liang, *Carbon dioxide capture from flue gas using regenerable sodium-based sorbents* [M], Louisiana State University and Agricultural & Mechanical College, 2003.



10 T. Nasiman and H. Kanoh, *Ind. Eng. Chem. Res.*, 2020, **59**, 3405–3412.

11 H. Luo and H. Kanoh, *J. Energy Chem.*, 2017, **26**, 972–983.

12 T. Cai, J. K. Johnson, Y. Wu and X. Chen, *ACS Appl. Mater. Interfaces*, 2019, **11**, 9033–9041.

13 C. Zhao, X. Chen, E. J. Anthony, X. Jiang, L. Duan, Y. Wu, W. Dong and C. Zhao, *Prog. Energy Combust. Sci.*, 2013, **39**, 515–534.

14 Y. Wu, Z. Lv, X. Zhou, J. Peng, Y. Tang and Z. Li, *Chem. Eng. J.*, 2019, **355**, 815–821.

15 Z. Zhou, L. Mei, C. Ma, F. Xu, J. Xiao, Q. Xia and Z. Li, *Chem. Eng. Sci.*, 2016, **147**, 109–117.

16 L. Mei, T. Jiang, X. Zhou, Y. Li, H. Wang and Z. Li, *Chem. Eng. J.*, 2017, **321**, 600–607.

17 F. Gao, S. Wang, G. Chen, J. Duan, J. Dong and W. Wang, *Adsorption*, 2020, **26**, 701–709.

18 Z. Refaat, M. E. Saied, A. Naga, S. A. Shaban, H. B. Hassan, M. R. Shehata and F. Y. E. Kady, *Environ. Sci. Pollut. Res. Int.*, 2023, **30**, 53817–53832.

19 M. Hefti, D. Marx, L. Joss and M. Mazzotti, *Microporous Mesoporous Mater.*, 2015, **215**, 215–228.

20 M. M. Almoneef, H. Jedli and M. Mbarek, *Mater. Res. Express*, 2021, **8**, 065602.

21 A. Heidari, H. Younesi, A. Rashidi and A. Ghoreyshi, *J. Taiwan Inst. Chem. Eng.*, 2014, **45**, 579–588.

22 J. McEwen, J.-D. Hayman and A. Ozgur Yazaydin, *Chem. Phys.*, 2013, **412**, 72–76.

23 G. Chen, F. Wang, S. Wang, C. Ji, W. Wang, J. Dong and F. Gao, *Korean J. Chem. Eng.*, 2021, **38**, 46–54.

